AIP | Journal of Applied Physics

Magnetization dynamics and ferromagnetic resonance behavior of melt spun FeBSiGe amorphous alloys

D. C. Estévez, I. Betancourt, and H. Montiel

Citation: J. Appl. Phys. **112**, 053923 (2012); doi: 10.1063/1.4752250
View online: http://dx.doi.org/10.1063/1.4752250
View Table of Contents: http://jap.aip.org/resource/1/JAPIAU/v112/i5
Published by the AIP Publishing LLC.

Magnetization dynamics and ferromagnetic resonance behavior of melt spun FeBSiGe amorphous alloys

D. C. Estévez,[1] I. Betancourt,[1,a)] and H. Montiel[2]
[1]*Departamento de Materiales Metálicos y Cerámicos, Instituto de Investigaciones en Materiales, Universidad Nacional Autónoma de México, Mexico, D.F. 04510, Mexico*
[2]*Centro de Ciencias Aplicadas y Desarrollo Tecnológico, Universidad Nacional Autónoma de México, Mexico, D.F. 04510, Mexico*

(Received 11 May 2012; accepted 9 August 2012; published online 14 September 2012)

Frequency-dependent magnetic properties of melt spun $Fe_{80}B_{10}Si_{10-x}Ge_x$ ($x = 0.0$–10.0) were studied by means of inductance spectroscopy (using the complex permeability formalism) and ferromagnetic resonance techniques. The magnetization dynamics showed two magnetization mechanisms, reversible bulging of domains and hysteresis. The dominant mechanism changed as Ge progressively replaced Si; the changes reflect the crystallization processes observed for higher Ge contents, $x > 5$. High relaxation frequencies (above 1 MHz) were observed for alloys with $x \geq 2.5$. In the ferromagnetic resonance response, coupling and decoupling between the amorphous and crystalline phases were detected depending on the orientation of the alloy samples. This allowed the calculation of the anisotropy fields of the alloys—the decreasing trend with increasing Ge content was interpreted in terms of a variable easy direction. © *2012 American Institute of Physics*. [http://dx.doi.org/10.1063/1.4752250]

INTRODUCTION

Amorphous magnetic alloys obtained as thin ribbons (with characteristic thickness below 30 μm and variable length) by rapid solidification techniques have been a subject of intense research since the 1980s, because their ultrasoft magnetic character allows interesting technological applications in devices for conversion of electromagnetic energy into mechanical energy and for signal processing. Other applications include: power electronics, electrical power conditioning, magnetic sensors, telecommunications, and automotive magnets.[1,2] In particular, FeBSi-based glassy alloys have been extensively studied for their excellent combination of physical properties, including high values of saturation magnetization, magnetic permeability, and Curie temperature, along with very low power losses[2–5] and, for specific formulations, outstanding mechanical performance.[6,7] On the other hand, for the study of soft magnetic materials, characterization of the magnetic permeability as a function of frequency is very important, because of the possibility of developing materials for high-frequency applications in telecommunications, wireless systems and radar detection, among others. In this context, a powerful characterization technique is impedance spectroscopy (ImS), which has been widely used to investigate electrical polarization phenomena in a variety of dielectric, ferroelectric, and piezoelectric materials.[8] By means of a simple change in experimental conditions (essentially using coils instead of electrodes to apply external ac magnetic fields h_{ac} of variable intensity and frequency), and by a convenient transformation of complex formalisms (inductances and magnetic permeabilities instead of capacitances and permittivities), "inductance spectroscopy" (InS) may be derived.[9] Within this framework, the dominant magnetization processes may be resolved by measuring across a wide frequency range. At low frequencies, all the magnetization processes (namely reversible domain wall (DW) bulging, domain wall displacement, spin rotation, and spin precession) contribute to the total permeability (and thus, the overall magnetization). However, they possess different dynamics in the sense that each magnetization process is characterized by a time-constant. As the frequency of h_{ac} increases, the magnetization processes with slow dynamics (i.e., large time-constants) become unable to follow the excitation field; they therefore exhibit dispersion, and thus a decrease in the total value of permeability occurs. The permeability value for each frequency range, the frequency at which a process ceases to follow the field, and the dispersion (where the behavior changes from being dominated by one magnetization process to another) are significant aspects of the frequency response of the material. A wide variety of magnetic materials have been investigated by InS, such as ferrites,[10] amorphous and nanocrystallized ribbons,[11] amorphous wires,[12] and glass-coated microwires.[13] Ferromagnetic resonance (FMR) is also a powerful technique to investigate magnetic phases in materials because it can determine magnetic parameters such as: magnetic anisotropy, resonant field, line width of absorption, and saturation magnetization,[14,15] as well as enable investigation of magnetic order by comparing measurements made of samples in different orientations to evaluate the contribution of magnetic anisotropy.[14]

Although there have been numerous reports regarding the impact of variations in chemical composition on the physical properties of FeBSi-based amorphous alloys (see Refs. 16–19 and references therein), very few studies have been performed concerning the influence of progressive additions of Ge on their magnetic properties, in spite of the beneficial effects of Ge—increasing the magnetic moment,[17] and improving the thermal stability of FeB-based amorphous

a)Author to whom correspondence should be addressed. Electronic mail: israelb@unam.mx. Tel.: +52 5556224654. Fax: +52 5556161371.

alloys through expansion of the supercooled liquid regions.[20] In this work, the systematic replacement of Si by Ge in the alloy system $Fe_{80}B_{10}Si_{10-x}Ge_x$ (x = 0.0–10.0 at. %) has been performed, and the influence Ge on the magnetization dynamics and the ferromagnetic resonance behavior has been determined.

EXPERIMENTAL TECHNIQUES

Metallic ribbons (20–30 μm thickness and 1.8 mm wide) for each composition of the alloy series $Fe_{80}B_{10}Si_{10-x}Ge_x$ (x = 0.0, 2.5, 5.0, 7.5, and 10.0 at. %) were produced by melt spinning into a sealed chamber under He atmosphere at a roller speed of 40 m/s. The microstructures of the as-cast alloys were determined by x-ray diffraction analysis (XRD) using a Siemens D5000 diffractometer with Co-K_α radiation. Magnetic permeability measurements were performed using an impedance analyzer HP 4192 A operating at frequencies between 5 Hz and 13 MHz, and are reported as complex permeability: $\mu^* = \mu_{re} + i\mu_{im}$ ($i = \sqrt{-1}$).[21] FMR measurements were made with a Jeol JES-RES 3X spectrometer operating at 9.4 GHz (X-band) using horizontal-parallel orientation, O1 (with the longitudinal axis of the ribbon parallel to the H_{dc} field and normal to the H_{ac} field) as well as vertical-parallel orientation, O2 (the longitudinal axis of the ribbon normal to the H_{dc} field and parallel to the H_{ac} field). For both cases, the magnetization lies along the longitudinal axis of the ribbon.

RESULTS

XRD diffractograms for all alloy ribbons are shown in Fig. 1. Lower Ge compositions (x = 0.0, 2.5, and 5.0) present a single broad peak around wave vector, $K_p = 4\pi\sin\theta/\lambda = 31.19\,nm^{-1}$, with no diffraction peaks corresponding to any crystalline phases; this is indicative of a fully glassy structure. By contrast, for samples with $x \geq 7.5$, some additional peaks are observed at $2\theta = 52.7°$ (x = 7.5) and at $2\theta = 52.48°$ and 77.18° (x = 10.0). The peaks near 52° are associated with the (110) and (220) planes of cubic $Fe_3(Si,Ge)$, whilst the peak at 77° corresponds to the (620) plane of Fe_3Ge phase, according to ICDD files 065-0994 and 03-065-9102. These diffraction peaks show that the alloy progressively crystallizes upon Ge substitution.

The real and imaginary components of complex permeability, μ_{re} (f) and μ_{im} (f) for the alloy series $Fe_{80}B_{10}Si_{10-x}Ge_x$ are shown in Fig. 2. These curves can be used to evaluate the active magnetization mechanisms across the frequency range for a given h_{ac} intensity.[21,22] For instance, for x = 0.0, the $\mu_{re}(f)$ plot measured at $h_{ac} = 0.42$ A/m shows plateau-like behavior for frequency f values up to 6×10^4 Hz. This shape of the μ_{re} curve can be attributed to reversible bulging of the magnetic DWs pinned at defects on the ribbon surface (such as voids, surface irregularities, and the very surface itself). Hence, μ_{re} at these frequencies is associated with the initial permeability of the material. Further increase in f causes a significant reduction in $\mu_{re}(f)$, which can be ascribed to a relaxation-type dispersion of the reversible bulging mechanism, once the DWs are no longer able to follow the ac magnetic variation. Beyond a threshold (or relaxation) frequency f_x, μ_{re} becomes very small, reflecting the contribution of spin rotation, which is the only magnetization process active for $f > f_x$.[21,22] As the Ge content x increases, an initial decrease in μ_{re} (from 800 to 650) is observed between x = 0.0 and x = 2.5, followed by an increase with Ge content up to x = 7.5. A distinct reduction (to $\mu_{re} = 200$) is recorded for x = 10.0.

Complementary information is obtained from the imaginary component μ_{im}, which is usually attributed to the magnetic losses within the alloy (such as hysteresis, eddy current, or power losses),[23,24] with the maximum in $\mu_{im}(f)$ found at f_x. This f_x displays an inverse behavior with

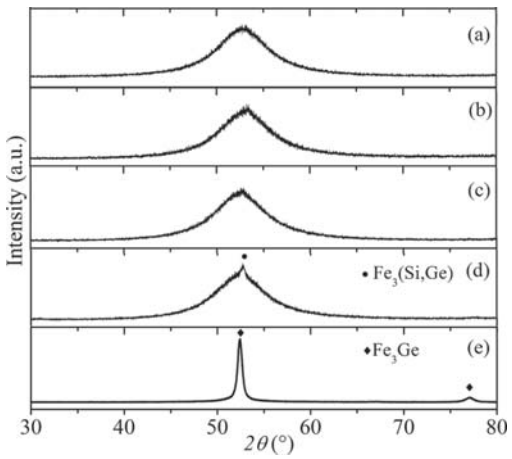

FIG. 1. XRD patterns for the alloy series $Fe_{80}B_{10}Si_{10-x}Ge_x$: (a) x = 0.0, (b) x = 2.5, (c) x = 5.0, (d) x = 7.5, (e) x = 10.0.

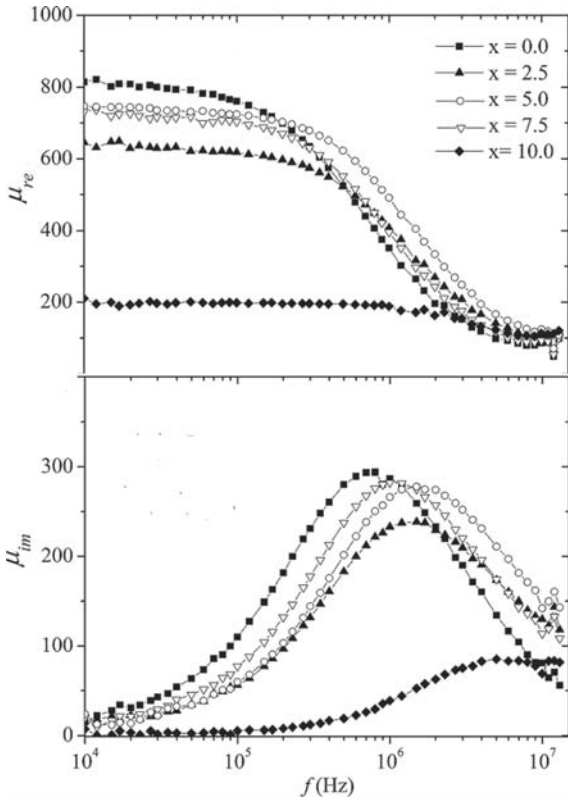

FIG. 2. Real and imaginary components $\mu_{re}(f)$, μ_{im} (f) of complex permeability for the alloy series $Fe_{80}B_{10}Si_{10-x}Ge_x$, for an *ac* applied field h_{ac} of 0.42 A/m.

increasing Ge concentration, showing values above 1 MHz for Ge-containing alloys. Further increase of the *ac* frequency of the magnetic applied field h_{ac} (into the GHz range) affords the resonance absorption, as described later in the ferromagnetic resonance section.

Different behavior is seen at the higher h_{ac} intensity of 1.69 A/m, where two features are seen in the μ_{re} (f) plot for $x = 0.0$ as shown in Fig. 3(a): the reversible bulging process together with its corresponding relaxation at $f > 1 \times 10^5$ Hz, and a significant increase in μ_{re} across the frequency interval 3×10^3 Hz $< f < 1 \times 10^5$ Hz, after μ_{re} (f) has been constant at $f < 3 \times 10^3$ Hz. This increment in μ_{re} can be interpreted in terms of a magnetization mechanism involving the irreversible displacement of DWs caused by the higher h_{ac} intensity.[21,25] The displacement of the DWs leads to a hysteresis process within the material, which also manifests as a relaxation-type dispersion (i.e., a change of process) across the frequency interval (3×10^3 Hz $< f < 1 \times 10^5$ Hz). A progressive decrease in μ_{re} with increasing f up to a threshold frequency is seen; this threshold frequency is termed the "hysteresis relaxation frequency" f_x^h. Beyond f_x^h, the irreversible displacement of DWs is no longer able to follow the changes in the h_{ac} excitation field, allowing reversible bulging (which has a shorter time constant) to become the active magnetization process.

The imaginary component μ_{im} (f) exhibits behavior consistent with the sequence of magnetization mechanisms described above, showing one maximum for each process, i.e., the irreversible displacement of DWs at f_x^h and the reversible bulging of DWs at f_x. In this case, $f_x^h = 8 \times 10^3$ Hz and $f_x = 8 \times 10^5$ Hz. The marked change in magnitude between both threshold frequencies ($f_x^h \ll f_x$) reflects the significant difference between the time constant for each magnetization mechanism. The time constant for the hysteresis process is much larger than that for the reversible bulging of DWs. In addition, the magnetic losses (which are proportional to the area under the μ_{im} curve) are also comparatively larger for the irreversible displacement of DWs than for the reversible bulging, because of the higher energy cost of the hysteresis process relative to that for reversible deformation of the DWs.

At higher Ge concentration ($x \geq 2.5$), the low time constant process (i.e., hysteresis) disappears, leaving reversible bulging of DWs as the only active mechanism. The effectiveness of this mechanism decreases progressively with increasing Ge content. As expected, the imaginary component $\mu_{im}(f)$ (Fig. 3(b)) also exhibits a transition from two peaks, corresponding to two magnetization processes, to a single maximum, associated with the magnetization mechanism with the higher time constant. The relaxation frequency f_x increases monotonically with increasing x, as indicated by the maxima in the $\mu_{im}(f)$ plots moving to higher frequencies. These results show a significant compositional influence on the time constant response of amorphous alloys via the effective magnetic anisotropy; a similar effect has also been observed in amorphous wires[26] and soft ferrites.[27]

The FMR spectra for the whole alloy ribbon series are shown in Figs. 4 and 5 for the O1 and O2 orientations, respectively. For O1 (Fig. 4), the alloy samples exhibit a main FMR absorption near 710 Oe for Ge contents of up to $x = 7.5$, which can be ascribed to the ferromagnetic amorphous matrix response. For the $x = 10.0$ sample, an additional absorption at 650 and 750 Oe overlaps the main response. This second absorption can be attributed to a secondary magnetic phase; the XRD results in Fig. 1 indicate that this is the crystalline Fe_3Ge phase. The O2 orientation spectra (Fig. 5) show similar features, with a main absorption associated with the amorphous phase, located between 900 and 1000 Oe, along with additional signals between 900 and 1200 Oe. The variation of the anisotropy field H_k with Ge content is shown in Fig. 6. This H_k was calculated according to the following expression:[28,29]

$$H_k \approx \frac{H_{Res}^{O2} - H_{Res}^{O1}}{2}, \quad (1)$$

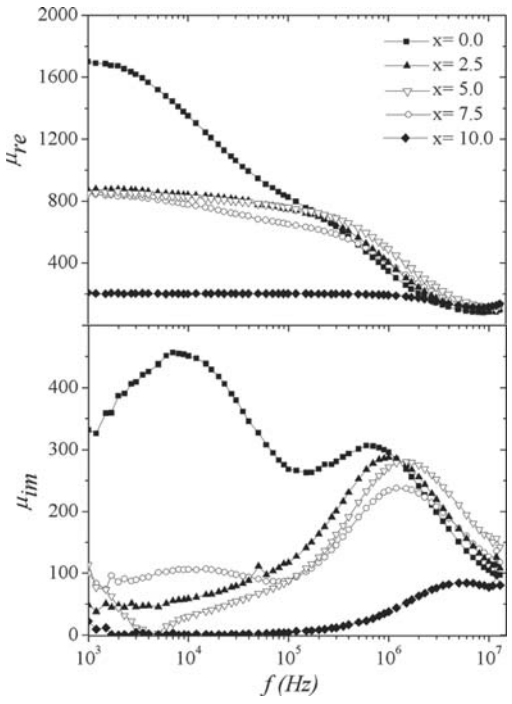

FIG. 3. Real and imaginary components $\mu_{re}(f)$, μ_{im} (f) of complex permeability for the alloy series $Fe_{80}B_{10}Si_{10-x}Ge_x$, for an *ac* applied field h_{ac} of 1.69 A/m.

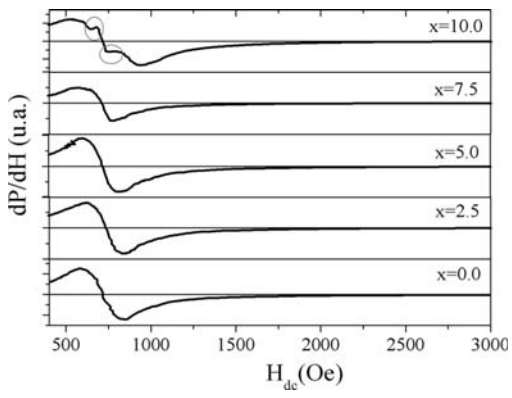

FIG. 4. FMR spectra for the alloy series $Fe_{80}B_{10}Si_{10-x}Ge_x$ (O1 orientation). The additional absorptions associated with crystalline phases are circled in red.

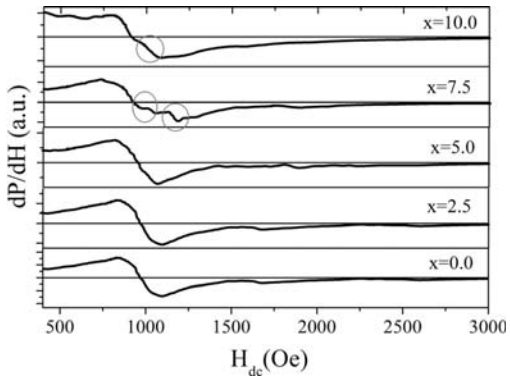

FIG. 5. FMR spectra for the alloy series $Fe_{80}B_{10}Si_{10-x}Ge_x$ (O2 orientation). The additional absorptions associated with crystalline phases are circled in red.

where H_{Res}^{O2} and H_{Res}^{O1} correspond to the resonance fields along O1 and O2 orientations, respectively (both fields were established from where the dP/dH = 0 line intersects the dP/dH versus H curve in each case).

The total magnetic anisotropy is made up of shape anisotropy (K_s, associated with the geometry of the ribbons), magnetoelastic anisotropy (K_m, caused by residual stresses induced during fabrication), and crystalline anisotropy (K_c, arising from the presence of crystalline Fe_3Ge). Bearing in mind that for both orientations O1 and O2, the magnetization lies along the longitudinal ribbon axis, it is expected that there will only be a marginal contribution of the shape anisotropy to the total anisotropy, and hence, the strong dependence of the internal field on H_k can be seen within the resonance absorption results. This behavior has been reported previously in equivalent Co-based amorphous alloys, for which a significant contribution of the shape anisotropy to H_k was found when the magnetization was directed outside the longitudinal axis of the ribbons.[30] For the O1 orientation, the resonant field (H_{res}) values are smaller than those for the O2 orientation, with the line-shapes reflecting the coupling between different magnetic phases, which in turn can be distinguished due to their different internal fields, as shown in Fig. 4 for the x = 10 sample. The difference between resonant fields along the O1 and O2 orientations confirms that the easy-axis of the magnetization is the longitudinal ribbon axis;

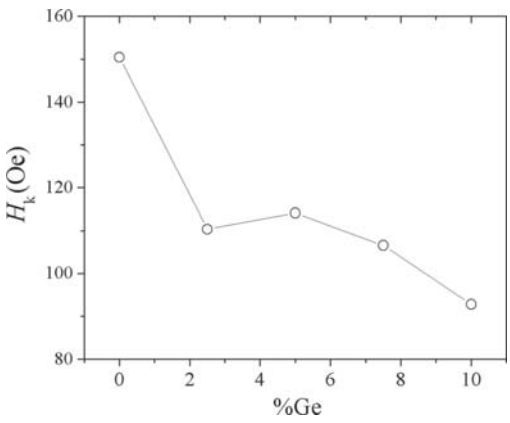

FIG. 6. The anisotropy field H_k as a function of Ge content x for the alloy series $Fe_{80}B_{10}Si_{10-x}Ge_x$.

additionally, coupling between magnetic phases is better along this direction.

DISCUSSION

For the lower Ge concentration values (up to x = 5.0), the alloy samples exhibited a fully glassy structure, as shown by XRD. The observed variations in the spectroscopic $\mu_{re}(f)$, and $\mu_{im}(f)$ curves can be explained on the basis that magnetic permeability, and thus the magnetization processes, are highly sensitive to the chemical composition of the alloy ribbons. The changes in the short-range atomic ordering introduced by alloying atoms can affect the exchange interaction between magnetic moments, as well as the formation of spin-up/spin-down bands.[5,31,32] For example, the decrease in μ_{re} observed for x = 2.5 can be attributed to a reduced magnetization saturation, M_s, which in turn may be associated with a preliminary change in the local coordination of magnetic atoms (such as an increase in packing density) affecting the magnetic moment per atom. Ge atoms have a 7.5% larger atom radius than Si, which also means that the radius difference for the Ge-B pair is 51.2%, noticeably larger than the 40.6% difference for the Si-B pair.[33] This contributes to the expansion of the amorphous structure with increasing Ge content; this expansion separates Fe-Fe pairs, yielding a less densely packed structure. This decrease in packing is associated with a recovery of the magnetic moment, and hence, of the permeability, as illustrated in Fig. 2, for x > 2.5. For x > 5.0, the observed variation in magnetic properties is correlated with the gradual precipitation of secondary crystalline phases induced by the increase in Ge:Si ratio. The significant reduction in relative permeability for the x = 10 sample is because of the increase in volume fraction of crystalline phase in this sample. These secondary phases provide numerous structural defects which can act as pinning centers, and in turn determine the marked decrease in $\mu_{re}(f)$ observed at the higher Ge concentrations (Fig. 2).

On the other hand, the FMR measurements along the O1 orientation are dominated by the behavior of the ferromagnetic amorphous matrix, which is manifested as a single absorption peak. The single peak response for the x = 7.5 sample reflects coupling between the various magnetic anisotropies present within the alloy, according to the Herzer model.[34] In contrast, for the x = 10.0 alloy, decoupling between the two resonant signals arises from the competition between magnetic anisotropies, with the magnetocrystalline contribution of the secondary phases playing a dominant role.

When we consider the O2 orientation, the higher resonant fields observed suggest that there is an easy direction of magnetization along the longitudinal ribbon axis. In addition, the changes in the modes of resonance can be ascribed to the fact that the magnetic anisotropy of the amorphous matrix is different compared to that of the crystalline phases, leading to decoupling between both signals. Conversely, since H_k comprises several contributions to the effective magnetic anisotropy—K_{eff}: the crystalline anisotropy (K_c, for alloys with Ge content x > 5.0); shape anisotropy (K_s, owing to the elongated geometry of the ribbons), and magnetoelastic anisotropy (K_m, caused by residual stresses induced during melt-spinning

and directed along the longitudinal ribbon axis)—the progressive decrease of H_k with the addition of Ge indicates that the easy axis for magnetization is moving away from the main ribbon axis. This movement is caused by the progressive reduction of the magnetoelastic term K_m as a result of a counterbalancing effect provoked by an increase in the number of randomly oriented crystals, which in turn promotes a decline of the effective anisotropy along the main ribbon axis. This reduction also affects the formation and dynamics of magnetic domains, as suggested by the evolution of the magnetization mechanism, shown in Fig. 3, from DW displacement to reversible bulging of pinned DWs.

CONCLUSIONS

The progressive replacement of Ge by Si in FeBSi melt spun amorphous alloys has a noticeable influence on their magnetization dynamics, affecting the reversible bulging of domains walls as well as the hysteresis mechanism, via the crystallization process observed at Ge contents above 5 at. %. Interesting relaxation frequencies above 1 MHz were observed for alloys with $x \geq 2.5$. In the FMR response, the coupling or decoupling between the amorphous and crystalline phases is dependent on the orientation of the samples, which is consistent with an easy direction along the longitudinal ribbon axis for $x = 0.0$, and deviation from this direction for higher Ge concentrations.

ACKNOWLEDGMENTS

The authors would like to thank Dr. G. Alvarez for the FMR measurements.

[1]R. Hasegawa, J. Magn. Magn. Mater. **215/216**, 240 (2000).
[2]H. Gavrila and V. Ionita, J. Optoelectron. Adv. Mater. **4**, 173 (2002).
[3]M. E. McHenry, M. A. Willard, and D. E. Laughlin, Prog. Mater. Sci. **44**, 291 (1999).
[4]R. B. Schwarz, T. D. Shen, U. Harms, and T. Lillo, J. Magn. Magn. Mater. **283**, 223 (2004).
[5]G. Herzer, "Amorphous and nanocrystalline materials," in *Concise Encyclopedia of Magnetic and Superconducting Materials*, 2nd ed., edited by K. H. J. Buschow (Elsevier, Amsterdam, 2005), p. 19.
[6]A. Inoue, B. L. Shen, A. R. Yavari, and A. L. Greer, J. Mater. Res. **18**, 1487 (2003).
[7]A. Inoue, B. L. Shen, and C. T. Chang, Acta Mater. **52**, 4093 (2004).
[8]E. Barsoukov and J. Ross Macdonald, *Impedance Spectroscopy. Theory, Experiment and Applications*, 2nd ed. (Wiley, Hoboken, 2005).
[9]R. Valenzuela, Mater. Res. Soc. Symp. Proc. **699**, R2.1 (2001).
[10]J. T. S. Irvine, E. Amano, A. Huanosta, R. Valenzuela, and A. R. West, Solid State Ionics **40/41**, 220 (1990).
[11]E. Amano, R. Valenzuela, J. T. S. Irvine, and A. R. West, J. Appl. Phys. **67**, 5589 (1990).
[12]C. Echavarrieta, P. Quintana, E. Amano, R. Valenzuela, J. González, N. Murillo, and J. M. Blanco, J. Magn. Magn. Mater. **140–144**, 1903 (1995).
[13]I. Betancourt and R. Valenzuela, J. Non-Cryst. Solids **329**, 155 (2003).
[14]M. Kuzminski, H. K. Lachowicz, L. Lezama, A. S. lawska-Waniewska, and J. M. Barandiarán, J. Non-Cryst. Solids **287**, 334 (2001).
[15]V. Siruguri and S. N. Kaul, J. Phys.: Condens. Matter **8**, 4567 (1996).
[16]F. E. Luborsky, J. J. Becker, J. L. Walter, and H. H. Lieberman, IEEE Trans. Magn. **15**, 1146 (1979).
[17]H. S. Chen, Rep. Prog. Phys. **43**, 353 (1980).
[18]A. Inoue, *Bulk Amorphous Alloys. Preparation and Fundamental Characteristics* (Trans Tech Publications Ltd, Switzerland, 1999).
[19]W. H. Wang, C. Dong, and C. H. Shek, Mater. Sci. Eng. R. **44**, 45 (2004).
[20]A. Inoue and J. S. Gook, Mater. Trans., JIM **36**, 1282 (1995).
[21]R. Valenzuela, J. Alloys Compd. **369**, 40 (2004).
[22]R. Valenzuela, H. Montiel, M. P. Gutiérrez, and I. Betancourt, J. Magn. Magn. Mater. **294**, 239 (2005).
[23]D. X. Chen and J. L. Muñoz, IEEE Trans. Magn. **35**, 1906 (1999).
[24]S. Chikazumi, *Physics of Magnetism* (Robert E. Krieger, New York, 1978).
[25]R. Valenzuela, Physica B **299**, 280 (2001).
[26]K. L. García and R. Valenzuela, IEEE Trans. Magn. **34**, 1162 (1998).
[27]R. Valenzuela and J. T. S. Irvine, J. Magn. Magn. Mater. **160**, 386 (1996).
[28]S. N. Kaul and V. Siruguri, J. Phys. Condens. Matter **4**, 505 (1992).
[29]K. Ounadjela, G. Suran, and F. Machizaud, Phys. Rev. B **40**, 578 (1989).
[30]H. Montiel, G. Alvarez, R. Zamorano, and R. Valenzuela, J. Non-Cryst. Solids **353**, 908 (2007).
[31]M. L. Fdez-Gubieda, A. García-Arribas, J. M. Barandiarán, R. López Antón, I. Orue, P. Gorria, S. Pizzini, and A. Fontaine, Phys. Rev. B **62**, 5746 (2000).
[32]J. M. Barandiarán, P. Gorria, I. Orúe, M. L. Fdez-Gubieda, F. Plazaola, and A. Hernando, Phys. Rev. B **54**, 3026 (1996).
[33]O. N. Senkov and D. B. Miracle, Mater. Res. Bull. **36**, 2183 (2001).
[34]G. Herzer, IEEE Trans. Magn. **25**, 3327 (1989).